McCue, Scott W. and Forbes, Lawrence K. (2002) Free surface flows emerging from beneath a semi-infinite plate with constant vorticity. *Journal of Fluid Mechanics* 461:pp. 387-407.

Free surface flows emerging from beneath a semi-infinite plate with constant vorticity

By SCOTT W. MCCUE† AND LAWRENCE K. FORBES‡
Department of Mathematics, University of Queensland, Queensland 4072, Australia

(Received 7 July 1999)

The free surface flow past a semi-infinite horizontal plate in a finite-depth fluid is considered. It is assumed that the fluid is incompressible and inviscid and that the flow approaches a uniform shear flow downstream. Exact relations are derived using conservation of mass and momentum for the case where the downstream free surface is flat. The complete nonlinear problem is solved numerically using a boundary integral method and these waveless solutions are shown to exist only when the height of the plate above the bottom is greater than the height of the uniform shear flow. Interesting results are found for various values of the constant vorticity. Solutions with downstream surface waves are also considered, and nonlinear results of this type are compared with linear results found previously. These solutions can be used to model the flow near the stern of a (two-dimensional) ship.

1. Introduction

In this paper, we consider the steady flow of an incompressible, inviscid fluid past a semi-infinite horizontal plate. Solutions to this problem that exhibit no waves on the downstream free surface can be used to model the flow emerging from a rectangular vessel (see figure 1). This configuration was examined by Vanden-Broeck & Keller (1987) in their study of irrotational weir flows. It was shown analytically, using conservation of mass and momentum, that when the plate is fixed at a particular height, there is only one possible solution. This behaviour is similar to that found in weir flows, where the upstream velocity is dependent on the geometry of the weir. A special limiting case of this problem was also considered by Benjamin (1968). Here the problem is that of an

† Present address: Division of Theoretical Mechanics, School of Mathematical Sciences, University of Nottingham, University Park, Nottingham NG7 2RD, UK.
‡ Present address: Department of Mathematics, University of Tasmania, GPO Box 252-37 Hobart 7001, Australia.

empty cavity displacing a fluid beneath a horizontal fixed boundary. Benjamin used this special limiting problem to model horizontally flowing gravity currents without viscosity or surface mixing.

The full nonlinear problem (of flow past a semi-infinite horizontal plate) without waves was examined by Asavanant & Vanden-Broeck (1996). They solved the problem numerically using a series truncation method for the case where the irrotational flow is supercritical (Froude number $F > 1$) downstream. The analytic results of Vanden-Broeck & Keller (1987) were verified using this numerical method. No subcritical (Froude number $F < 1$) solutions were considered.

In § 2 of this paper, we extend the results of Vanden-Broeck & Keller (1987), Benjamin (1968) and Asavanant & Vanden-Broeck (1996) to allow the fluid to possess a constant vorticity ω throughout, so that there is a uniform shear flow with height H and velocity $c + \omega y$ far downstream. The constant vorticity could be created by friction acting on the bottom boundary, or perhaps by wind on the free surface.

It turns out that the problem depends on the three nondimensional parameters

$$F = c/\sqrt{gH}; \qquad \Omega = \omega H/c; \qquad \gamma = D/H. \tag{1.1}$$

Here F is the Froude number, which is a measure of the downstream velocity at $y = 0$, g is the acceleration due to gravity, Ω is the nondimensional vorticity, and D and γ are the dimensional and nondimensional heights of the plate above the horizontal bottom respectively.

It is shown using conservation of mass and momentum that there is a one-parameter family of solutions for each vorticity value in the range $-1 < \Omega < 0.31$ whose behaviour is qualitatively the same as the irrotational ($\Omega = 0$) family described by Vanden-Broeck & Keller (1987). These solutions bifurcate from the uniform shear flow ($\gamma = 1$) at the critical Froude number $F = 1/\sqrt{1 + \Omega}$. As the height of the plate γ increases from 1, the Froude number also increases, until a limiting configuration is reached where the free surface detaches from the plate at a stagnation point.

For each vorticity value $\Omega > 0.31$, there is also a family of solutions which bifurcate from the uniform shear flow. However, for these families there is no physical limit as the Froude number increases, and in fact the solutions exist for Froude numbers up to and including $F = \infty$. From the mathematical point of view, this solution branch continues even further, until the height of the plate $\gamma \to \infty$. The corresponding Froude

numbers, however, take imaginary values in this case, and hence these solutions lack physical significance.

There is an additional branch of solutions for $0 < \Omega < 0.31$ which do not bifurcate from a uniform shear. These solutions have the same behaviour in the limit $\gamma \to \infty$ as the solutions for $\Omega > 0.31$ described above. As γ decreases, the solutions approach a limiting configuration where the free surface detaches from the plate at a stagnation point. Therefore, there are two limiting configurations for vorticity values in the range $0 < \Omega < 0.31$ where the velocity vanishes at the detachment point.

The complete nonlinear problem is reformulated in § 2.2 using Cauchy's integral formula. The numerical method used to solve the problem is described in § 2.3, while the results are presented in § 2.4.

Section 3 of this paper is concerned with solutions to the problem that are characterized by a train of waves downstream on the free surface (see figure 8). Here the problem can be used to model the flow near the stern of a ship. McCue & Stump (2000) solved the linear problem exactly using the Wiener-Hopf technique under the assumption that the nondimensional height of the plate above the bottom γ is close to one. In this case, the waves on the free surface approach small-amplitude sine waves far downstream. Vanden-Broeck (1980) considered the special case where the fluid depth was infinite. He derived exact results of the nonlinear problem and also presented some numerical solutions. Both of these studies are restricted to the case where the flow is irrotational ($\Omega = 0$).

It is shown in § 3.1 that the extension of McCue & Stump's results to allow for a constant vorticity is essentially trivial. The numerical method used to solve the nonlinear problem is given in § 3.2 and the results are presented in § 3.3. The Froude number here is an input parameter, and is not found as part of the solution process, unlike in § 2. It is shown that when the draught parameter $\epsilon = 1 - \gamma$ is small, the computed nonlinear solutions agree with the linear results of McCue & Stump (2000). However, as ϵ increases, the downstream waves become more nonlinear in shape, with sharp crests and broad troughs. It is expected that these waves will ultimately break when the crests of the waves reach the stagnation level, which is given by Bernoulli's equation.

We note here that constant vorticity has been included in the infinite-depth problem recently by Kang & Vanden-Broeck (in press). They present analytical results for linear waves using conservation laws as well as some numerical solutions to the nonlinear problem. The analysis in § 3 is an extention of that given in Kang & Vanden-Broeck

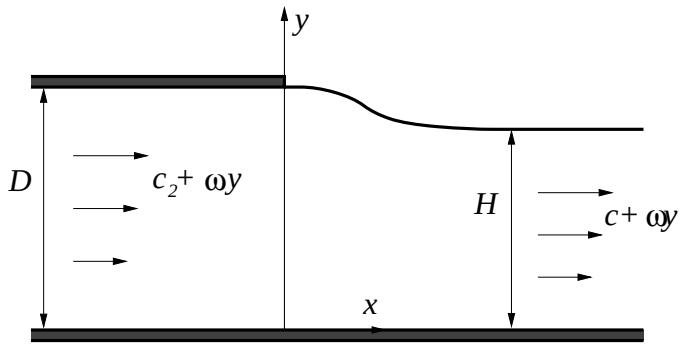

FIGURE 1. A definition sketch in dimensional variables of the waveless free surface flow past a semi-infinite flat plate.

(in press) to a fluid of finite depth, for which the constant vorticity in the flow has a natural physical interpretation in terms of the shear arising from bottom friction. As a consequence, we also avoid any potential difficulties with constant vorticity at infinite depth.

2. Solutions with no waves downstream

2.1. *Conservation of mass and momentum*

Consider the steady two-dimensional free surface flow under a semi-infinite horizontal plate, as shown in figure 1. The fluid is assumed to be inviscid and incompressible, and for this study it is assumed that there is a constant vorticity ω throughout the flow region. Cartesian coordinates are chosen so that the x-axis lies on the horizontal bottom, and the y-axis points vertically upwards. With this choice of coordinates, the free-surface detaches from the plate at the point $(x, y) = (0, D)$. Far downstream, the flow approaches a uniform shear flow with height H and horizontal velocity $c + \omega y$.

It can be shown that since the vorticity is constant, Bernoulli's equation takes the form

$$\tfrac{1}{2}(u^2 + v^2) + gy + \frac{p}{\rho} - \omega\psi = \tfrac{1}{2}(c + \omega H)^2 + gH \tag{2.1}$$

throughout the flow field. Here, u and v are the x and y components of the velocity vector $\mathbf{q}$, p is the fluid pressure, ρ is the density of the fluid, and ψ is the streamfunction, which has been set to zero on the free surface and plate. A conservation of mass argument can be used to show that if the horizontal velocity of the fluid approaches $c_2 + \omega y$ far

upstream under the plate, then

$$c_2 = \frac{1}{D}\left[cH + \tfrac{1}{2}\omega(H^2 - D^2)\right]. \tag{2.2}$$

Following Vanden-Broeck & Keller (1987), we integrate the x component of Euler's equation over the flow domain, to give

$$\iint \left[u\frac{\partial u}{\partial x} + v\frac{\partial u}{\partial y} + \frac{1}{\rho}\frac{\partial p}{\partial x}\right] \mathrm{d}S = \iint \left[\operatorname{div}\mathbf{f} - u\operatorname{div}\mathbf{q}\right] \mathrm{d}S = 0,$$

where $\mathbf{f} = (u^2 + p/\rho + gy)\,\mathbf{i} + uv\,\mathbf{j}$. Here $\mathbf{i}$ and $\mathbf{j}$ are the usual unit vectors in the x and y direction respectively. But since the flow is incompressible, $\operatorname{div}\mathbf{q} = 0$, and hence after the use of the divergence theorem, we obtain the line integral

$$\int_\Gamma \left[u(\mathbf{q}\cdot\mathbf{n}) + (p/\rho + gy)n_x\right] \mathrm{d}l = 0, \tag{2.3}$$

where Γ is a (non-oriented) curve along the boundary of the flow region. The vector $\mathbf{n}$ is an outward pointing unit vector normal to Γ, and n_x is the x component of this vector.

It is easy to see that there are no contributions to the integral in (2.3) from the horizontal bottom and horizontal plate, since both $\mathbf{q}\cdot\mathbf{n}$ and n_x vanish there. Along the free surface we have set $p = 0$, so the contribution along this segment becomes

$$\int_H^D gy\,\mathrm{d}y = g(D^2 - H^2)/2.$$

That leaves us to consider the two vertical lines at $x = \pm\infty$. For these contributions, the term $p/\rho + gy$ is found using Bernoulli's equation (2.1). It follows that, after some algebra, these two contributions to the integral in (2.3) become $c^2H/2 - \omega^2H^3/6 + H(c + \omega H)^2/2 + gH^2$ and $-c_2^2D/2 + \omega^2D^3/6 - D(c + \omega H)^2/2 - gDH$. Adding all these terms together, we finally obtain, after more algebra, the equation

$$\frac{(H-D)^2}{D}\left[c^2 - gD + c\,\omega H + \frac{\omega^2}{12}(3H^2 - 2HD - D^2)\right] = 0.$$

Here we have used the expression in (2.2) to eliminate c_2.

Evidently, there are two possibilities. The first of these is trivial. That is, $H = D$, and there is a uniform shear flow throughout. The second possibility is that there are two-parameter families of solutions where, in non-dimensional variables, the Froude number is given by

$$F^2 = \frac{\gamma}{1 + \Omega + \Omega^2(3 - 2\gamma - \gamma^2)/12}. \tag{2.4}$$

Thus, for every fixed value of γ and Ω, there is only one solution. From here on we will only be considering nondimensional variables.

For each nondimensional vorticity value Ω, there is a family of solutions given by (2.4)

which bifurcates from the uniform shear flow when $\gamma = 1$. The corresponding Froude number is $F = 1/\sqrt{1+\Omega}$, which is also the critical Froude number found from linear theory (see McCue & Forbes 1999). When $\gamma < 1$, the formula (2.4) predicts that the downstream flow is subcritical. However, numerical evidence (see § 2.4) suggests that these flows may not exist. The only reliable solutions computed are those with $\gamma > 1$, and these are all supercritical flows.

When the vorticity $\Omega = 0$, the flow is irrotational, and the expression (2.4) reduces to $F^2 = \gamma$, which is exactly the result found by Vanden-Broeck & Keller (1987). Irrotational solutions exist for values of γ in the range $1 \leq \gamma \leq 2$. The solution for $\gamma = 2$ is a limiting solution, at which a stagnation point forms where the free surface detaches from the plate. The angle of detachment becomes 120°, as predicted by Dagan & Tulin (1972). This configuration was first considered by Benjamin (1968), in his study of gravity currents. Benjamin argued that the basic properties of horizontal gravity currents could be explored by ignoring viscosity and fluid mixing, and supposing there is a fixed upper boundary at a finite distance above the horizontal bottom. The resulting problem is equivalent to that of a wedge of fluid displacing a heavier fluid from the under side of a horizontal boundary. Without any loss of generality the gravity constant can be rescaled and it can be assumed that the density of the lighter fluid is negligible. We are left with the current limiting configuration with $\gamma = 2$, which is an empty cavity propagating steadily along the upper boundary of a fluid.

Benjamin describes another simple interpretation for this limiting configuration. Imagine a semi-infinite, rectangular shaped tube filled with a fluid. Now suppose the tube is held in a horizontal position and the end of the tube is suddenly removed. The fluid will flow out of the tube under the action of gravity and form some sort of jet (see figure 4 in Benjamin's paper). After a long time a steady state will be reached in the vicinity of the point where the free surface intersects the upper boundary of the tube. This point is the stagnation point in our limiting configuration (with $\gamma = 2$).

The parameters for which solutions with non-zero vorticity in this limiting configuration exist can be found by considering the following form of Bernoulli's equation

$$\tfrac{1}{2}(u^2 + v^2) + \frac{1}{F^2} y = \tfrac{1}{2}(1+\Omega)^2 + \frac{1}{F^2}, \tag{2.5}$$

which holds on the free surface only. At the stagnation point, $y = \gamma$ and both u and v

vanish. Therefore these solutions exist only when

$$F^2 = \frac{2(\gamma - 1)}{(1 + \Omega)^2}.$$

Equating this expression with the one in (2.4) gives a quadratic equation for Ω, with the solutions

$$\Omega = \frac{-6 \pm (\gamma - 1)\sqrt{6\gamma\,(\gamma + 1)}}{3 + \gamma + \gamma^2 + \gamma^3}. \tag{2.6}$$

We will examine these limiting solutions in more detail later in § 2.4. For now we mention these solutions generalize those found by Benjamin (1968), by allowing the fluid to have constant vorticity throughout. They can be used to describe the flow out one end of a rectangular shaped tube, with the constant vorticity modelling the real situation where friction acting on the bottom boundary causes some sort of shear in the flow. However they are no longer applicable to gravity currents, as the argument used by Benjamin only holds for irrotational flow.

2.2. *Boundary integral formulation*

We now present the boundary integral method used to solve the problem described in § 2.1. This method is very similar to that used in the past by many authors (for example, see Vanden-Broeck 1994; Forbes & Belward 1996; McCue & Forbes 1999; and McCue & Forbes 2001), and hence it will only be described briefly here.

The flow is rotational, and hence is governed by Poisson's equation $\nabla^2\psi = \Omega$ throughout the flow domain. Since the vorticity Ω is constant, we can write the streamfunction as

$$\psi(x, y) = y + \tfrac{1}{2}\Omega y^2 + \Psi(x, y), \tag{2.7}$$

so that the introduced function Ψ satisfies Laplace's equation. It follows that the complex quantity

$$f(z) = \Phi(x, y) + \mathrm{i}\Psi(x, y) \tag{2.8}$$

is an analytic function of $z = x + \mathrm{i}y$. The real function Φ, which is the harmonic conjugate of Ψ, also satisfies Laplace's equation in the flow domain.

The two components of the velocity vector can be found from (2.7), and are written in the form

$$u(x, y) = 1 + \Omega y + U(x, y), \qquad v(x, y) = V(x, y), \tag{2.9}$$

where

$$U = \frac{\partial \Psi}{\partial y} = \frac{\partial \Phi}{\partial x}, \qquad V = -\frac{\partial \Psi}{\partial x} = \frac{\partial \Phi}{\partial y}. \tag{2.10}$$

The analytic function

$$\chi(z) = \frac{\mathrm{d}f}{\mathrm{d}z} = U - \mathrm{i}V \tag{2.11}$$

must therefore vanish far downstream, since the flow approaches a uniform shear there.

It is convenient to write each point on the horizontal plate and free surface as $(x(s), y(s))$, where the parameter s is a measure of arclength. We set $s = 0$ at the detachment point, so that $(x(s), y(s)) = (s, \gamma)$ on the plate. The derivatives of $x(s)$ and $y(s)$ on the free surface are related by the arclength condition

$$x'(s)^2 + y'(s)^2 = 1, \tag{2.12}$$

for $s > 0$.

Applying Cauchy's integral formula to the function χ defined by (2.11), we obtain the integral equation

$$\oint_{\Gamma} \frac{\chi(z(t))z'(t)}{z(t) - z(s)}\,\mathrm{d}t = 0. \tag{2.13}$$

Here the curve Γ is a closed path in the physical plane consisting of the free surface and horizontal plate, except for the point $(x(s), y(s))$, which is by-passed with a vanishingly small semi-circle, the reflected free surface and plate about the horizontal bottom, and two connecting vertical lines at $x = \pm\infty$.

The contribution to the integral in (2.13) from the vertical line at $x = \infty$ is evidently zero, since the function χ is zero there. It can be shown that the contribution from the vertical line at $x = -\infty$ is also zero, although the function χ approaches some real constant as $x \to -\infty$ (see McCue & Forbes 1999 for details). Finally, the contribution from the semi-circle is $-\mathrm{i}\pi\chi(z(s))$. Taking the imaginary part of (2.13), and using the symmetry of the reflected flow with respect to the x-axis, we obtain, after some algebra, the required integral equation

$$\begin{aligned} \pi U(s) = &\int\!\!\!\!\!\!-_{-\infty}^{\infty} \frac{\Phi'(t)(y(t) - y(s)) - \Psi'(t)(x(t) - x(s))}{(x(t) - x(s))^2 + (y(t) - y(s))^2}\,\mathrm{d}t \\ &+ \int_{-\infty}^{\infty} \frac{\Phi'(t)(y(t) + y(s)) - \Psi'(t)(x(t) - x(s))}{(x(t) - x(s))^2 + (y(t) + y(s))^2}\,\mathrm{d}t, \end{aligned} \tag{2.14}$$

where $\Phi'(t) = U(t)x'(t) + V(t)y'(t)$ and $\Psi'(t) = -V(t)x'(t) + U(t)y'(t)$. The first integral in (2.14) is a Cauchy principle value integral.

The boundary conditions are now considered. Bernoulli's equation (2.5) expresses the

fact that the pressure is constant on the free surface. The condition that fluid cannot pass through the free surface and plate can be satisfied by noting that $\mathrm{d}\psi/\mathrm{d}s = 0$ there. It follows from (2.7) that

$$\Psi'(s) = -(1 + \Omega y(s))y'(s) \tag{2.15}$$

for all values of s. Finally, the condition of no vertical velocity on the horizontal bottom is automatically satisfied by the integral equation (2.14), since the preceding derivation involves the reflection of the flow about the x-axis.

2.3. *Numerical method*

Our goal is to solve the integral equation (2.14) for the unknown functions $x(s)$, $y(s)$, $U(s)$ and $V(s)$ aswell as the parameter F, subject to the conditions (2.5), (2.12) and (2.15). To do this, we need to place a mesh of grid points over the free surface and plate. It is desirable for this problem that the grid points are clustered near the detachment point at $(x(0), y(0)) = (0, \gamma)$; thus, following McCue & Forbes (2001), we introduce the transformation

$$\xi = \begin{cases} -\ln(1-s), & s < 0 \\ \ln(1+s), & s \geq 0. \end{cases}$$

A mesh of N evenly spaced grid points $\xi_1, \xi_2, \ldots, \xi_{na}, \ldots, \xi_N$ is now placed over the new variable ξ. The point $\xi_{na} = 0$ is chosen to represent the detachment point, so that the points $\xi_1, \ldots, \xi_{na}$ lie on the horizontal plate, and the points $\xi_{na}, \ldots, \xi_N$ lie on the free surface. We choose N to always be an odd integer so that the value of na can be set to $na = (N+1)/2$. The first grid point ξ_1 and last grid point ξ_N are supposed to represent $-\infty$ and ∞ respectively.

An initial guess is made for the vector of $(3N+3)/2$ unknowns

$$\boldsymbol{u} = [y'_{na}, \ldots, y'_N; \Phi'_1, \ldots, \Phi'_N; F]^T,$$

and all other flow quantities are calculated in the following way. The x'_i on the free surface are found from the arclength condition (2.12), which can be rewritten in terms of the new variable ξ as

$$x'(\xi)^2 + y'(\xi)^2 = e^{2|\xi|}. \tag{2.16}$$

A backward trapezoidal rule is used to compute the x_i and y_i on the free surface, given that $x_{na} = 0$ and $y_{na} = \gamma$, and the Ψ'_i are found using the kinematic condition (2.15). On the plate, $x_i = 1 - \exp(-\xi_i)$, $y_i = \gamma$, $x'_i = \exp(-\xi_i)$ and $y'_i = 0$. Finally, the velocities

U_i and V_i are found from

$$U(\xi) = [x'(\xi)\Phi'(\xi) + y'(\xi)\Psi'(\xi)]e^{-2|\xi|}$$
$$V(\xi) = [y'(\xi)\Phi'(\xi) - x'(\xi)\Psi'(\xi)]e^{-2|\xi|}.$$

Bernoulli's equation (2.5) is now satisfied at the na grid points $\xi_{na}, \ldots, \xi_N$ and the integral equation (2.14) is satisfied at the $N-1$ half-mesh points $\xi_{j+1/2}$, $j = 1, \ldots, N-1$. Trapezoidal rule integration is used to compute the integrals in (2.14). The singularity in the Cauchy principle value integral can be ignored, since the integral is evaluated exactly half way between consecutive mesh points. Linear interpolation is used to estimate the flow variables $x_{j+1/2}$, $y_{j+1/2}$ and $U_{j+1/2}$ at the half-mesh points. Since the domain of integration has been truncated, it is important to consider the contributions to the integrals in (2.14) that are ignored. The details of this estimation are straightforward, and can be found in McCue & Forbes (1999) and McCue & Forbes (2001).

We now have $(3N-1)/2$ equations for the vector of $(3N+3)/2$ unknowns $\boldsymbol{u}$. There are two more conditions to be satisfied. The first condition forces the free surface to detach smoothly from the horizontal plate, and this is satisfied by imposing $y'_{na} = 0$. The other equation enforces $y'_N = 0$, since the downstream free surface is flat. This system of equations is solved using a damped Newton's method.

Typically, when $1 < \gamma < 3$, $N = 501$ grid points were used on the free surface and flat plate with the arclength of the truncation point chosen to be $s_N = 10$. The corresponding mesh spacing in the new variable is about $\Delta\xi = 0.01$. For solutions with larger values of γ more grid points were used as needed, keeping the mesh spacing constant. We note here that the use of uneven grid points is not necessary, and that the same results can (in principle) be gained using an evenly spaced mesh. However many more grid points are needed to obtain well converged solutions when the mesh is evenly spaced, and hence valuable computing time can saved by using the method described in this subsection.

2.4. *Results*

As stated earlier in § 1 and § 2.1, there are families of solutions for each vorticity $\Omega > -1$ that bifurcate from the uniform shear current when $\gamma = 1$ and $F = 1/\sqrt{1+\Omega}$. The dependence of the Froude number F on the plate height γ for some of these families is shown in figure 2. The solid curves represent the analytic results given by (2.4), while the solid circles represent the values computed using the numerical method described in the previous subsection.

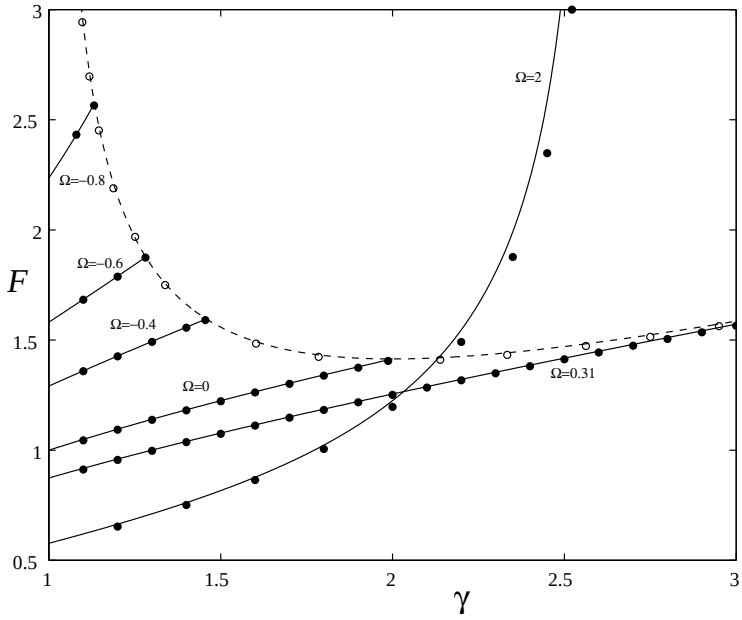

FIGURE 2. The dependence of the Froude number F on the plate height γ for six different values of the vorticity $\Omega = -0.8$, -0.6, -0.4, 0, 0.31 and 2. The solid lines indicate exact data, while the solid circles indicate computed data. Also included is the limiting curve for vorticity values in the range $-1 < \Omega < 0.31$. The exact data for this curve is indicated by the dashed line, while the open circles indicate computed data.

Also shown in figure 2 is the limiting curve, which is indicated by the dashed line. This exact data is found using the expression (2.6) (with the + sign) in conjunction with (2.4). All solutions on this curve are in the limiting configuration with a stagnation point where the free surface leaves the plate. The angle of detachment here is 120°. The open circles represent the computed Froude numbers found using a variation of the numerical scheme given in § 2.3. In this altered scheme, the equation $y'_{na} = 0$ is replaced by $y'_{na} = \sqrt{3}/2$. Also, one of the parameters γ or Ω becomes an extra unknown, so that the condition that the plate is located at the stagnation height can be enforced.

Figure 2 shows that for each $-1 < \Omega < 0.31$, solutions exist for values of γ until the limiting configuration is reached. Typical free surface profiles for a vorticity value in this range are shown in figure 3(a). The vorticity value chosen here is $\Omega = 0.2$. In the profiles for the lowest two γ values, the detachment is smooth. However, the profile for the highest γ value is in the limiting configuration, and the detachment here is at 120°. The contents of figure 3(b) will be explained later in this subsection.

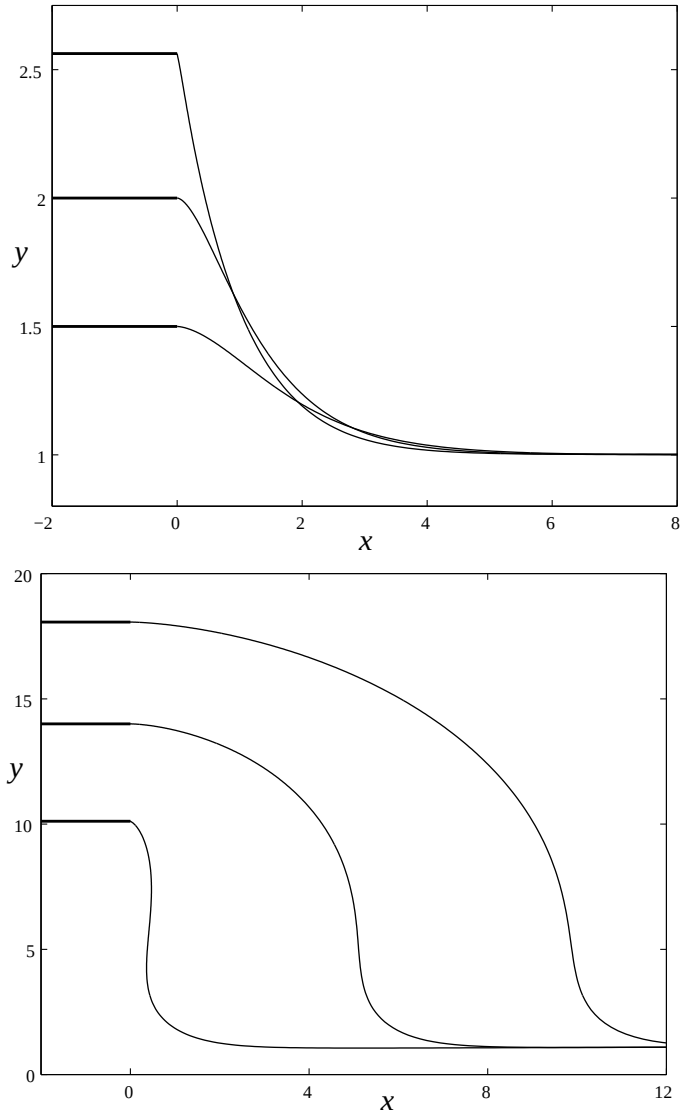

FIGURE 3. Typical free surface profiles are shown for $\Omega = 0.2$. In (a), the profiles from bottom to top are found for plate heights $\gamma = 1.5$, 2 and 2.56 and the corresponding calculated Froude numbers are $F = 1.12$, 1.30 and 1.47. In (b), the profiles from bottom to top are found for plate heights $\gamma = 10.11$, 14 and 18.07 and the corresponding calculated Froude numbers are $F = 3.56$, 5.50 and ∞.

The curve in figure 2 for $\Omega = 2$ is typical of all the curves for $\Omega > 0.31$. Here solutions exist for all Froude numbers up to and including $F = \infty$. For vorticity values in this range, there is no limiting configuration. This implies that the geometry considered by Benjamin (1968) (which models the flow out of one end of a semi-infinite box) cannot occur if $\Omega > 0.31$. Some free surface profiles for $\Omega = 2$ are shown in figure 4(a). Notice

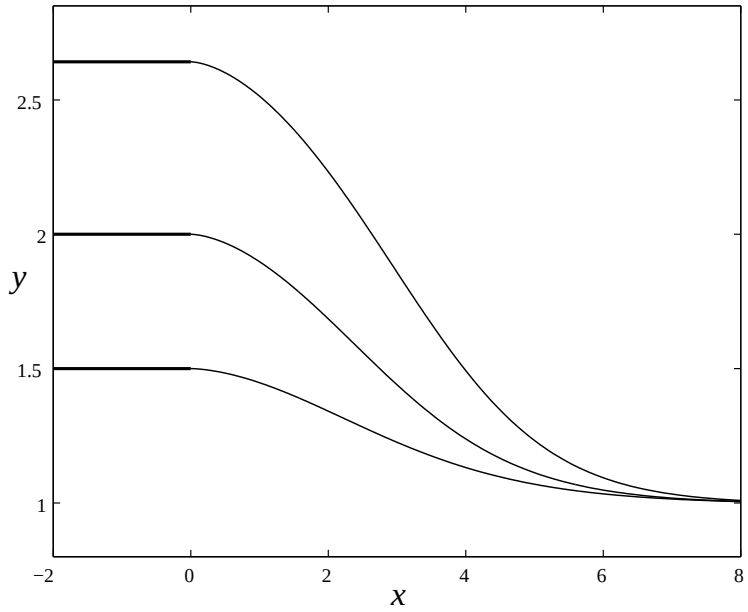

FIGURE 4. Typical free surface profiles are shown for $\Omega = 2$. The profiles from bottom to top are found for plate heights $\gamma = 1.5$, 2 and 2.64 and the corresponding calculated Froude numbers are $F = 0.81$, 1.20 and ∞.

how the elevation of the free surfaces approach the level $y = 1$ more slowly for this vorticity value than in the corresponding plots shown in figure 3(a), where the vorticity parameter is smaller. The mathematical branch of solutions for $\Omega = 2$ can be taken further, by allowing gravity to act upwards (here the Froude number must take imaginary values). Solutions of this type, which are clearly not physically possible, can be found for arbitrarily large values of γ.

Figure 5 shows the dependence of the Froude number F on the vorticity Ω for five different heights of the plate above the bottom $\gamma = 1$, 1.5, 2, 3 and 4. This figure should be viewed conjunction with figure 2. Again, as with figure 2, the solid lines represent the exact data given by the relation (2.4), and the solid circles represent the data found numerically. The dashed line represents the location of solutions in the limiting configuration. This limiting curve approaches $F = \infty$ as $\Omega \to -1$. As Ω increases from -1 on this curve, the Froude number F decreases until $\Omega = 0$ (here $\gamma = 2$ and $F = \sqrt{2}$), and then increases until $\Omega = 0.31$ (here $\gamma = 4.21$ and $F = 1.93$). At this point, the limiting curve undergoes a fold bifurcation, and then approaches $F = \infty$ as $\Omega \to 0$ from above. So for vorticity values in the range $0 < \Omega < 0.31$, there are two distinct solutions which are in the limiting configuration with a 120° angle at the point of detachment.

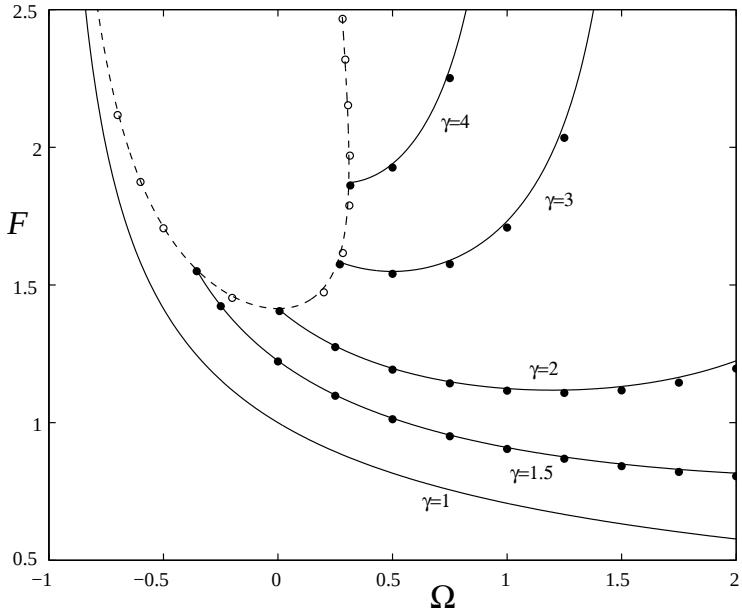

FIGURE 5. The dependence of the Froude number F on the vorticity Ω for five different plate heights $\gamma = 1$, 1.5, 2, 3 and 4. The solid lines indicate exact data, while the solid circles indicate computed data. Also included is the exact limiting curve, which is indicated by the dashed line. The computed data for this curve is indicated by the open circles.

New families of solutions for $0 < \Omega < 0.31$ can be found by starting with solutions on the upper branch of the limiting curve in figure 5, and increasing the plate height γ. An example of such a family is shown in figure 3(b), where typical free surface profiles for $\Omega = 0.2$ are shown. The profile with the lowest value of γ represents a solution on the upper fold of the limiting curve. As γ increases, the Froude number increases, until $F = \infty$. Finally, just as before with the families of solutions for $\Omega > 0.31$, the plate height γ could (in principle) be increased even further, if we allow gravity to act upwards, but these (unphysical) solutions are not presented here.

A characteristic of the limiting solution shown in figure 3(b) is that the free surface has an overhanging portion near $x = 0$. Solutions of this type could not be computed with the numerical scheme described in § 2.3, since the derivatives $x'(\xi)$ are not always positive. Instead, a variation of the scheme had to be used, where the variables $x'_{na}, \ldots, x'_N$ were added to the vector of unknowns and the arclength condition (2.16) was satisfied at the grid points $\xi_{na}, \ldots, \xi_N$.

Typical free surface profiles for solutions on the upper fold of the limiting curve in

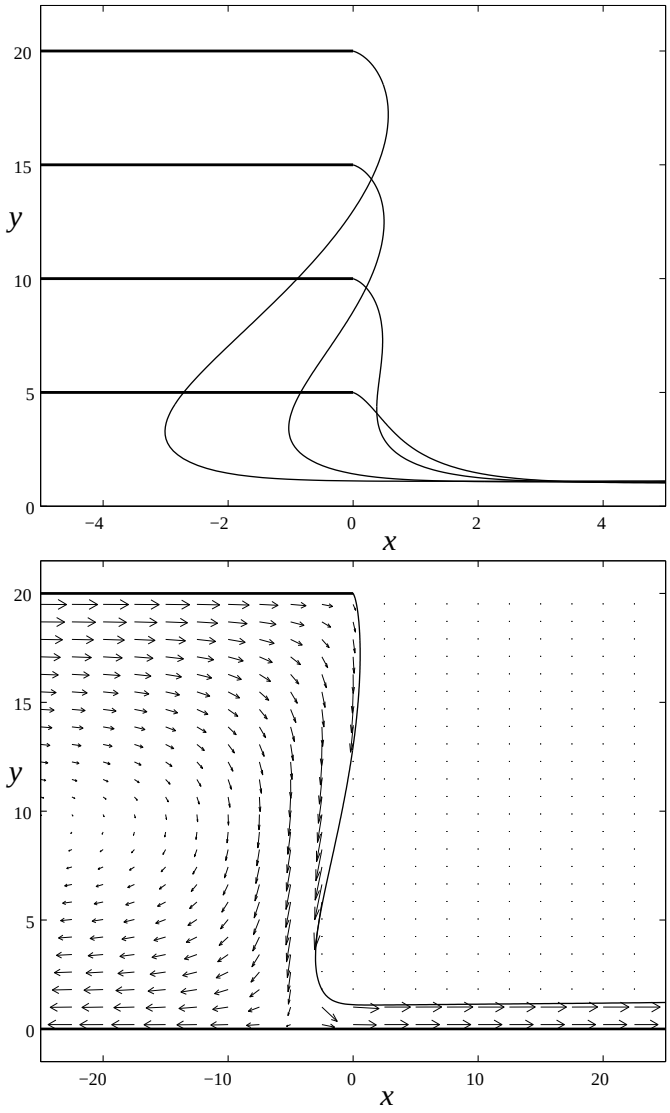

FIGURE 6. Typical free surface profiles for solutions on the upper fold of the limiting curve shown in figure 5. (*a*) Profiles from bottom to top are found for plate heights $\gamma = 5$, 10, 15 and 20. The corresponding calculated vorticity values and Froude numbers are $\Omega = 0.305$, $F = 2.17$; $\Omega = 0.202$, $F = 3.53$; $\Omega = 0.145$, $F = 4.62$; and $\Omega = 0.112$, $F = 5.54$ respectively. (*b*) Internal flow behaviour for the solutions with plate height $\gamma = 20$.

figure 5 are shown in figure 6(*a*). Note that the solutions for $\gamma = 10$, 15 and 20 all have overhanging portions of the free surface. This property is common to all solutions on the upper fold with vorticity values in the approximate range $0 < \Omega < 0.22$.

The boundary integral method currently used yields a solution which consists of all relevant information on the free surface and plate. Given this information, the velocity

field at each point in the flow domain can be calculated using Cauchy's integral formula. The resulting expression for the horizontal component $U(x, y)$ is the same as that given in (2.14), except that the coordinates on the free surface $x(s)$ and $y(s)$ are now replaced with the internal coordinates, and the term $\pi U(s)$ on the left hand side is replaced with $2\pi U(x, y)$. The formula for $V(x, y)$ is obtained in a similar way, by taking the real part of (2.13).

The internal flow behaviour for a solution with a large plate height γ is shown in figure 6(b). This solution is the same as the upmost profile shown in figure 6(a). An interesting feature of this flow field is that the horizontal velocity at the height $y = 0$ is negative far upstream under the plate. There must exist a dividing streamline which attaches to a stagnation point on the bottom. The fluid above the dividing streamline ultimately flows to the right of this stagnation point, and joins the uniform shear downstream as $x \to \infty$. The rest of the incoming fluid changes direction and flows back out under the plate as $x \to -\infty$. This feature occurs for extreme solutions with plate heights $\gamma > \sqrt{2/\Omega + 1}$, as indicated by (2.2). Another interpretation of this geometry (that doesn't involve negative horizontal velocities) arises by replacing the dividing streamline with a solid boundary. The result is flow out of a vessel with a semi-infinite obstruction on the bottom.

The solutions with infinite Froude number form a continuous one-parameter family which approaches the uniform shear flow as the vorticity $\Omega \to \infty$. As the plate height increases to infinity, the vorticity decreases monotonically to zero. Typical free surface profiles for $F = \infty$ are shown in figure 7. The profile for $\gamma = 30$ is multi-valued, as are all profiles for solutions on this branch with vorticity values in the range $0 < \Omega < 0.18$.

In this discussion of the results, we have presented numerical solutions to the current problem which are characterized by free surface profiles with overhanging portions (for example, the solutions on the upper fold of the limiting curve in figure 5 with $0 < \Omega < 0.22$ and the infinite Froude number solutions with $0 < \Omega < 0.18$). This phenomenon has been encountered in other problems with constant vorticity, especially those concerned with periodic or solitary waves (see, for example, Simmen & Saffman 1985; Teles da Silva & Peregrine 1988; and Vanden-Broeck 1994). These solutions may possibly be unstable to small perturbations, since they involve heavy fluid (water) overlying a lighter fluid (air).

With the help of Bernoulli's equation (2.1) we can use numerical solutions to compute values of the pressure underneath the plate. What is found is that as the x-coordinate

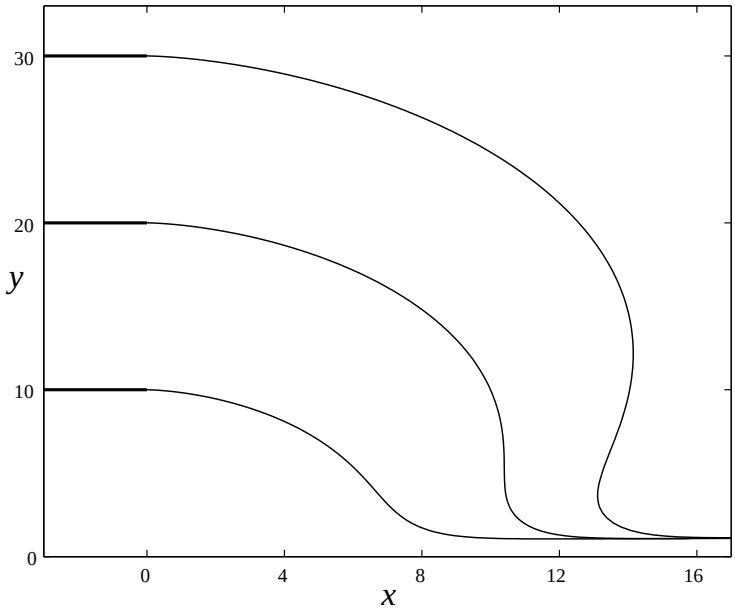

FIGURE 7. Typical free surface profiles are shown for $F = \infty$. The profiles from bottom to top are found for plate heights $\gamma = 10$, 20 and 30. The corresponding vorticity values are $\Omega = 0.376$, 0.181 and 0.119.

decreases along the plate from $x = 0$ the pressure rapidly decreases (from zero), and then asymptotes to a constant value. The exact value of this constant is given in nondimensional variables by

$$\lim_{x\to-\infty} p(x,\gamma) = -\frac{(\gamma-1)^2}{2\gamma^2}\left[1+\Omega+\frac{1}{12}\Omega^2(3+\gamma^2)\right],$$

and can easily be determined by combining equations (2.1), (2.2) and (2.4).

It should be noted that some waveless solutions with $\gamma < 1$ could be computed; however these were found to be unreliable. The reason for this unreliability is that the computed free surface profiles were heavily dependent on the truncation point ξ_N. Profiles with larger truncation points approached the level $y = 1$ more slowly than profiles with smaller truncation points. Furthermore, the computed Froude numbers for all these solutions did not agree with the analytic results given by (2.4). If waveless solutions for $\gamma < 1$ did in fact exist, and the current numerical method was able to compute them, then the resulting solutions should be independent of the grid used. Also, it is reasonable to expect that the computed Froude numbers would agree as well with the exact data for $\gamma < 1$ as they do for $\gamma > 1$. This is not the case. On the basis of this numerical evidence, we therefore

disregard the waveless solutions computed for $\gamma < 1$, and leave the question of whether such solutions really exist unanswered.

In § 2.1, it was shown that limiting solutions with stagnant detachment have vorticity values given by (2.6). The limiting solutions considered so far in this section correspond to the plus sign in (2.6), as stated earlier. Taking the minus sign yields a completely new branch of solutions in the limiting configuration, which exists for vorticity values in the range $-1 < \Omega < 0$. In the limit $\Omega \to -1$ on this new limiting branch, the plate height $\gamma \to 1$, and the Froude number $F \to \infty$, just like the first limiting branch examined earlier. As Ω increases from -1, the Froude number decreases until $\Omega = -0.50$ (here $\gamma = 3.38$ and $F = 4.40$), and then increases until $F \to \infty$, as $\Omega \to 0$.

The analysis in § 2.1 predicts that there are new families of solutions for each vorticity value $-1 < \Omega < 0$ which start on this new limiting curve and progress for larger values of γ until $F = \infty$. These new families are completely disjoint from all the other families considered in this section. Unfortunately, however, after much effort, none of these new solutions could be found numerically. Therefore, the question of whether these new families of solutions really do exist has to be left unanswered.

3. Solutions with downstream waves

In § 2.1, exact relations between the Froude number F, the vorticity Ω and the height of the plate above the bottom γ were derived under the assumption that the downstream free surface is flat. If there are waves on the free surface, then these relations are no longer valid, and the nature of the solutions is completely different. It is the purpose of this section to study the branch of solutions that are characterized by waves on the free surface.

3.1. *Linear solution*

As in § 2, we consider the free surface flow past a horizontal plate. However, as stated above, we now want to investigate solutions that exhibit waves on the downstream free surface (see figure 8). Solutions to this problem can be used to model the flow near the stern of a ship. We begin this investigation by considering a linear approximation to the nonlinear problem.

Upstream, under the plate, the flow is a uniform shear with horizontal velocity $c^* + \Omega\, y$ and height γ. It is convenient for this linear study to introduce the draught parameter ϵ,

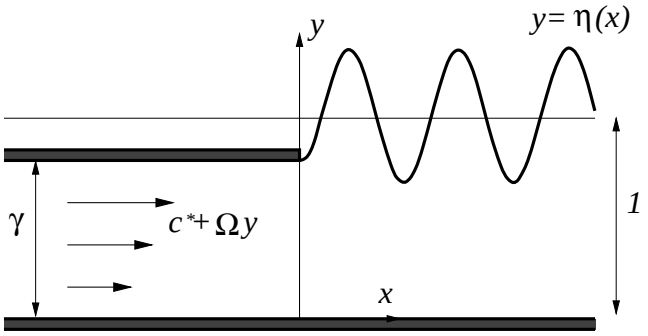

FIGURE 8. A definition sketch in nondimensional variables of the flow past a semi-infinite flat plate with waves on the free surface.

defined by

$$\epsilon = \gamma - 1,$$

so the problem becomes trivial when $\epsilon = 0$. The velocity c^* is the nondimensional version of c_2 defined in (2.2), and is given by

$$c^* = \frac{1}{1-\epsilon}\left[1 + \Omega\epsilon - \tfrac{1}{2}\Omega\epsilon^2\right].$$

The problem is governed by Poisson's equation for the streamfunction ψ. We write

$$\psi = c^* y + \tfrac{1}{2}\Omega y^2 + \Psi^*,$$

and the new function Ψ^*, along with its harmonic conjugate Φ^*, satisfy Laplace's equation. The velocity components can be calculated from Φ^* using the expressions

$$u = c^* + \Omega y + \frac{\partial \Phi^*}{\partial x}, \qquad v = \frac{\partial \Phi^*}{\partial y}.$$

The boundary conditions are the same as before. On the free surface, which will be denoted by $y = \eta(x)$, Bernoulli's equation (2.5) and the kinematic condition (2.15) apply. However in this section we rewrite the kinematic condition in the form

$$v = u\frac{\mathrm{d}\eta}{\mathrm{d}x}, \quad \text{on} \quad y = \eta(x). \tag{3.1}$$

The other two boundary conditions are $v = 0$ on $y = 0$ for $-\infty < x < \infty$, and $v = 0$ on $y = \gamma$ for $x < 0$.

We now assume that the draught of the plate ϵ is small, and introduce the perturbation expansions

$$\Phi^*(x, y) = \epsilon\,\phi(x, y) + O(\epsilon^2),$$

$$\eta(x) = 1 + \epsilon\,\eta_1(x) + O(\epsilon^2)\,.$$

When these perturbations are substituted into Laplace's equation $\nabla^2\Phi^* = 0$ and the boundary conditions, the resulting $O(\epsilon)$ problem reduces to solving Laplace's equation

$$\nabla^2\phi = 0 \qquad \text{for} \quad -\infty < x < \infty, \quad 0 < y < 1\,, \tag{3.2}$$

subject to the boundary conditions

$$\frac{\partial\phi}{\partial y} = 0 \qquad \text{on} \quad y = 1, \quad x < 0\,, \tag{3.3}$$

$$\frac{\partial\phi}{\partial y} - \left[\frac{F^2(1+\Omega)^2}{F^2\Omega(1+\Omega)+1}\right]\frac{\partial^2\phi}{\partial y^2} = 0 \qquad \text{on} \quad y = 1, \quad x > 0\,, \tag{3.4}$$

$$\frac{\partial\phi}{\partial y} = 0 \qquad \text{on} \quad y = 0 \quad -\infty < x < \infty\,. \tag{3.5}$$

There is also the detachment condition,

$$\frac{\partial\phi}{\partial x}(0,1) = \frac{1 - F^2(1+\Omega^2)}{F^2(1+\Omega)}\,. \tag{3.6}$$

This condition ensures that the free surface detaches from the plate at the correct height. Finally, given the solution to this problem, the location of the free surface can be found from the formula

$$\eta_1(x) = -\left[\frac{F^2(1+\Omega)}{F^2\Omega(1+\Omega)+1}\right]\left[1 + \Omega + \frac{\partial\phi}{\partial x}(x,1)\right], \tag{3.7}$$

for $x > 0$.

Linear theory tells us that when the Froude number $F < 1/\sqrt{1+\Omega}$, there are real roots of the dispersion relation

$$\frac{\tanh k}{k} = \frac{F^2(1+\Omega)^2}{F^2\Omega(1+\Omega)+1} = \hat{F}^2, \tag{3.8}$$

and small-amplitude waves are possible on the free surface. We denote these roots by $k = \pm\mu_R$. In this situation, the flow is called subcritical, and the parameter $\hat{F}$ defined in (3.8), takes values in the range $0 < \hat{F} < 1$. This parameter can be thought of as a modified Froude number. There are also infinitely many imaginary roots of (3.8), and these are denoted by $k = \pm\mathrm{i}\pi\mu_m$, for $m = 1, 2, \ldots$.

The linear problem described by (3.2)–(3.7) is essentially the same as that treated by McCue & Stump (2000), who considered the irrotational version of the problem. Allowing the flow to possess a constant vorticity throughout ultimately only affects the constants in equations (3.4), (3.6) and (3.7). After carefully working through the solution process of McCue & Stump (2000) with the new (but similar) conditions (3.3)–(3.7), it can be

shown that the location of the free surface becomes

$$\eta(x) = 1 + \epsilon\, K_1\, \frac{\cosh \mu_R}{T(\mu_R)T(-\mu_R)}\, \mathrm{Re}\left\{ T(\mu_R)\, \Gamma\left(1 - \frac{\mathrm{i}\mu_R}{\pi}\right) \Gamma\left(\frac{3}{2} + \frac{\mathrm{i}\mu_R}{\pi}\right) e^{\mathrm{i}\mu_R x} \right\}$$

$$+\epsilon\, K_2 \sum_{m=1}^{\infty} \frac{\mu_m T(\mathrm{i}\pi\mu_m)\Gamma(\mu_m) e^{-\pi\mu_m x}}{(\frac{1}{2} + \mu_m)[1 - \hat{F}^2 + \pi^2 \mu_m^2 \hat{F}^4]\Gamma(\frac{1}{2} + \mu_m)}, \tag{3.9}$$

where the constants K_1 and K_2 are given by

$$K_1 = -\frac{\hat{F}\sqrt{\pi(1 - \hat{F}^2)}}{\mu_R}, \qquad K_2 = \mu_R \hat{F}^3 \sqrt{\frac{1 - \hat{F}^2}{\pi}},$$

and the function $T(k)$ is an infinite product, defined by

$$T(k) = \prod_{n=1}^{\infty} \left[1 - \frac{n + 1/2 - \mu_n}{n + 1/2 - \mathrm{i}k/\pi}\right].$$

Full details are given in McCue (1999). Evidently, the linear solution for the location of the free surface does not depend on both the parameters F and Ω independently, but in fact only depends on the combination $\hat{F}$ (defined by (3.8)).

The $O(\epsilon)$ part of the free surface profile described by (3.9) has two distinct terms. The first term represents a sine wave with wavelength $\lambda = 2\pi/\mu_R$, and amplitude

$$A = \epsilon \hat{F} \sqrt{\frac{2(1 - \hat{F}^2)}{\hat{F}^2 + \mu_R^2 \hat{F}^4 - 1}}\,. \tag{3.10}$$

The second term is an infinite sum that decays exponentially as $x \to \infty$. The results of this subsection will be compared with the nonlinear results in § 3.3.

3.2. *Numerical method*

We describe here the numerical method used to solve the complete nonlinear problem with waves on the downstream free surface. The formulation is the same for this problem as that presented in § 2.2, and the only difference is in the numerical method. We emphasize here that all solutions presented in this section are computed for subcritical Froude numbers $F < 1/\sqrt{1 + \Omega}$ (or $\hat{F} < 1$).

Since we are seeking solutions with waves downstream, it is no longer desirable to use a mesh where the grid points are clustered near the detachment point. We therefore place a mesh of N equally spaced grid points $s_1, s_2, \ldots, s_{na}, \ldots, s_N$ over the arclength variable s on the horizontal plate and free surface. The points s_1 and s_N approximate $-\infty$ and ∞ respectively. The middle point $s_{na} = 0$ is chosen to represent the detachment point, where again we have set $na = (N + 1)/2$.

In this section the Froude number F is an input variable (as suggested by the linear

theory), and is not found as part of the solution process. It is therefore not included in the vector of $(3N+1)/2$ unknowns

$$\boldsymbol{u} = [y'_{na}, \ldots, y'_N; \Phi'_1, \ldots, \Phi'_N]^T.$$

With an initial guess of this unknown vector, all other flow quantities can be calculated in a similar way to that described in § 2.3.

The required $(3N+1)/2$ nonlinear equations consist of the integral equation (2.14), evaluated at the $N-1$ half-mesh points $s_{j+1/2}$, $j = 1, \ldots, N-1$, Bernoulli's equation evaluated at na grid points $s_{na}, \ldots, s_N$, and the condition of smooth detachment $y'_{na} = 0$. The integrals in (2.14) are treated the same way as in § 2.3. Note that we no longer force the free surface to be flat downstream.

3.3. *Results*

We begin our analysis of the numerical solutions by considering the special case where the flow is irrotational and the vorticity $\Omega = 0$. When the height of the plate $\gamma = 1$, the solution is simply the trivial uniform stream throughout. For values of γ close to 1, the solutions are characterized by a train of sinusoidal waves downstream, as indicated by the linear theory. A typical free surface profile for $\gamma \approx 1$ is shown in figure 9(a), where $\gamma = 0.999$, $F = 0.5$ and $\Omega = 0$. Here the actual grid points are shown as circles. The linear solution is also presented, and this is shown as a dashed line. For these parameters, both solution profiles are in excellent agreement.

As the horizontal plate is moved further from the undisturbed level, the amplitude of the downstream waves increases while the wavelength decreases. The waves themselves begin to develop sharp crests and broad troughs. This behaviour was found to continue until the elevation of the wave crests was close to the stagnation level $y_s = F^2(1+\Omega)^2/2 + 1$. At this stage the numerical method would not converge. It is expected that if the plate is moved even further away from the level $y = 1$, then the waves will approach the Stokes limiting configuration with 120° angles at the crests. The free surface profile shown in figure 9(b) represents the solution computed with the lowest value of γ when the Froude number and vorticity were fixed at $F = 0.5$ and $\Omega = 0$ respectively. Again, the actual grid points are shown as circles, while the profile found from linear theory is indicated by the dashed line. Notice how these two profiles are no longer in agreement.

The nonlinear solution presented in figure 9(a) was computed with $N = 601$ grid points on the free surface and body. The arclength of the last grid point was set $s_N = 8.06$. For

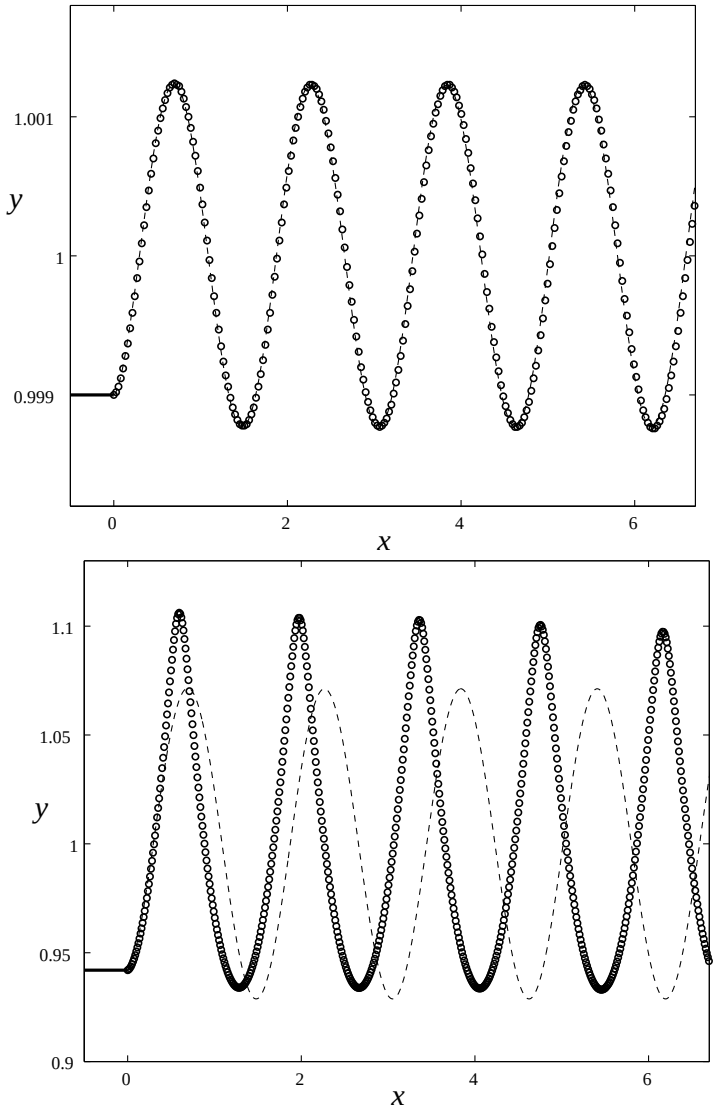

FIGURE 9. Typical free surface profiles are shown for $\Omega = 0$ and $F = 0.5$. The circles represent the actual grid points used in the computed solution, while the dashed line indicates the linear profile. The profiles in (a) are for $\gamma = 0.999$, while the profiles in (b) are for $\gamma = 0.942$.

solutions with distinctly non-sinusoidal free surface profiles, more grid points are needed to resolve the sharp crests. For example, $N = 1201$ grid points were used to compute the profile shown in figure 9(b) with $s_N = 7.45$.

It should be noted that the numerical method can yield solutions for $\gamma > 1$, in addition to solutions for $\gamma < 1$. The solutions for $\gamma > 1$ can no longer be used to model the flow near the stern of a ship, since the bottom of a ship can never be higher than the level

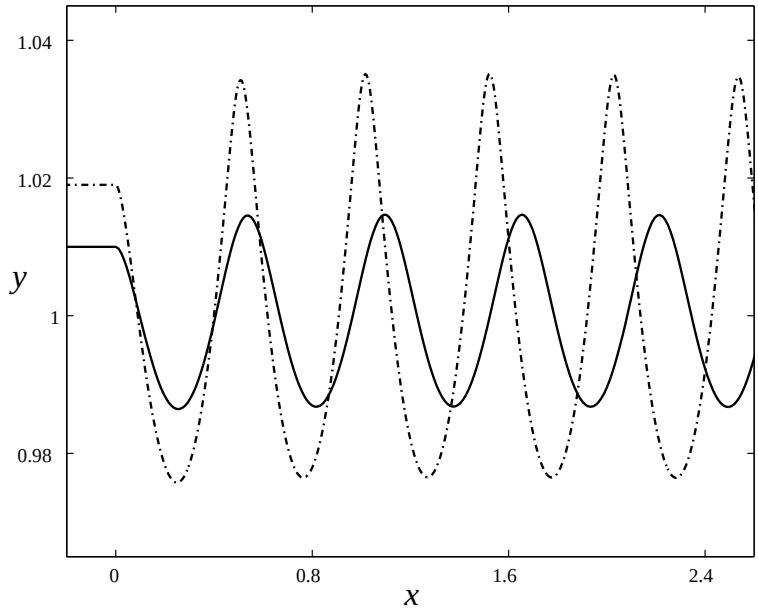

FIGURE 10. Typical free surface profiles for $\Omega = 0$, $F = 0.3$ and $\gamma > 1$. The solid profile corresponds to $\gamma = 1.01$ and the dot-dashed profile corresponds to $\gamma = 1.019$.

of the undisturbed free surface in a steady situation. However, these solutions can still model the flow emerging from a rectangular vessel. The difference between these flows and the ones considered in § 2 is that they are subcritical downstream, while those considered in § 2 are supercritical downstream.

A feature of the solutions examined in this section is that the free surface profiles computed for negative values of $\epsilon = 1 - \gamma$ with small magnitude are simply a reflection about the level $y = 1$ of the profiles found for ϵ values small and positive, but with the same magnitude. As $|\epsilon|$ increases, however, the profiles become non-sinusoidal and this symmetry no longer holds. Examples of free surface profiles calculated with $\gamma > 1$ are shown in figure 10. The solid profile was computed with $\gamma = 1.01$, while the dot-dashed profile was computed with $\gamma = 1.019$. In both cases the Froude number $F = 0.3$ and the vorticity $\Omega = 0$.

Figures 11(a) and 11(b) show the relationship between the steepness S of the downstream waves (defined to be the difference between the heights of the crests and the troughs divided by the wavelength) and the height of the plate γ for five different Froude numbers $F = 0.3$, 0.4, 0.5, 0.6 and 0.7, when the vorticity $\Omega = 0$. Figure 11(a) is for $\gamma \leq 1$ and figure 11(b) is for $\gamma \geq 1$. The linear steepness is indicated by the straight dashed lines, while the computed nonlinear data is indicated by the solid circles. In each

case, the upmost circle on the curves represents the most extreme solutions found using the current numerical scheme. For this range of Froude numbers, the maximum possible steepness for nonlinear water waves is $S = 0.14$ (see Cokelet 1977). One can estimate the upper and lower bounds of γ for each fixed Froude number by extrapolating the curves in figure 11 until they reach this maximum value. In reality, when $\gamma < 1$, it is not likely that the downstream waves ever quite reach the Stokes limiting configuration, since the elevation of the crest closest to the plate is generally the highest, and hence it will reach the stagnation level before the other crests. The result would be some sort of unsteady breaking wave, which cannot be computed with the current numerical method, since we restrict ourselves to steady flow.

Another feature of figure 11 is that for a fixed plate height γ, the steepness S of the downstream waves increases as the Froude number F decreases. This is mainly due to the fact that the wavelength contracts significantly as F decreases. A consequence of this wavelength contraction is that it becomes computationally expensive to calculate solutions accurately for small Froude numbers, since the mesh has to be fine enough to cover each wavelength adequately with sufficient grid points.

We now consider the effect vorticity has on the solutions. The dependence of the wave steepness S on the plate height γ is shown in figure 12 for three different vorticity values $\Omega = -0.4$, $\Omega = 0$ and $\Omega = 0.4$ when the Froude number is fixed to $F = 0.5$. It can be seen that the behaviour of the solutions for non-zero vorticity is qualitatively the same as that for irrotational flow. Also, this figure shows that the steepness S increases as the vorticity Ω decreases when the plate height γ and Froude number F are fixed. As in figure 11, the steepness predicted by the linear theory of § 3.1 is indicated by the dashed line. This linear steepness follows the nonlinear data quite closely, at least for values of γ near unity.

The linear theory presented in § 3.1 predicts that when the height of the plate $\gamma \approx 1$, all solutions with the same value of the parameter $\hat{F}$ have identical free surface profiles. This turns out to be true for all vorticity values except those near $\Omega = -1$. For example, solutions for $\gamma = 0.99$ were computed for different values of the vorticity Ω, keeping the parameter $\hat{F}$ constant at $\hat{F} = 0.5$. It was found that all solutions computed for vorticity values greater than about $\Omega = -0.7$ (keeping $\hat{F}$ constant at 0.5) had free surface profiles that were graphically indistinguishable from the linear profile. However, as the vorticity decreased from $\Omega = -0.7$, the shape of the free surface was found to

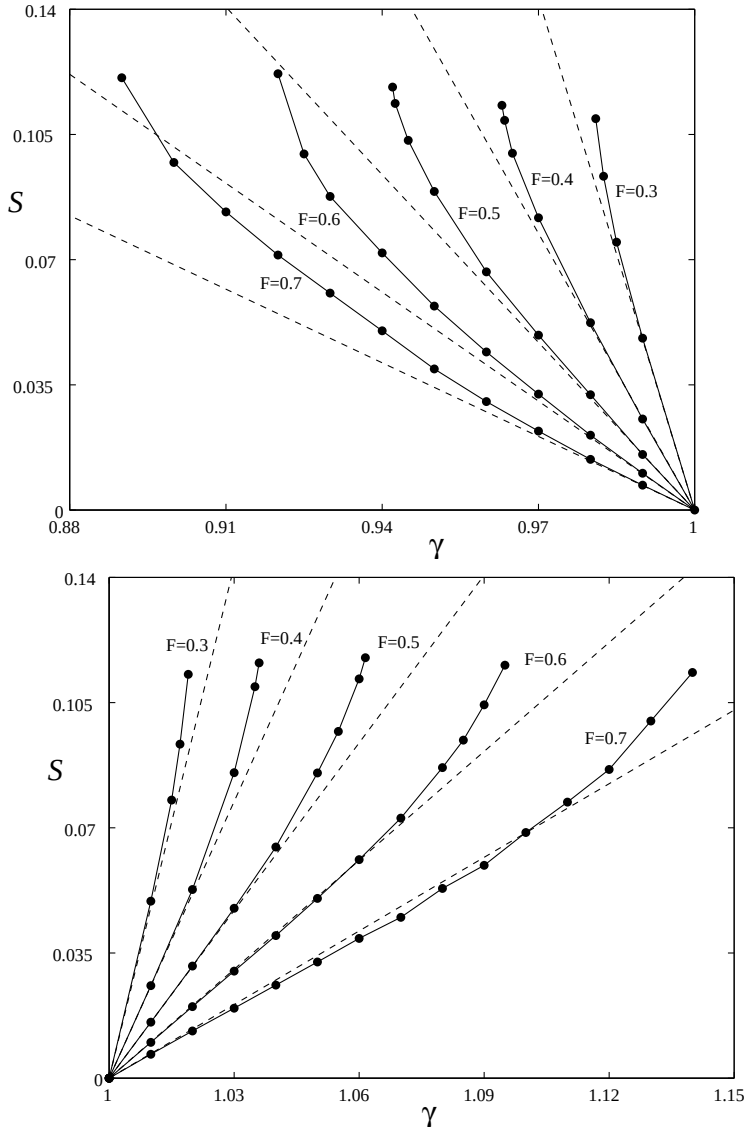

FIGURE 11. The dependence of the wave steepness S on the height of the plate γ for five different Froude numbers $F = 0.3$, 0.4, 0.5, 0.6 and 0.7 when the vorticity $\Omega = 0$. The computed data is shown with the solid circles, while the linear steepness is shown with the dashed lines. (a) is for $\gamma \leq 1$, and (b) is for $\gamma \geq 1$.

exhibit nonlinear characteristics such as broad troughs and sharp crests. Figure 13(a) shows two solution profiles for $\gamma = 0.99$ and $\hat{F} = 0.5$. The solution for $\Omega = -0.94$ and $F = 3.758$ is the one computed with the lowest vorticity value. It is expected that when the vorticity is decreased even further than this, the waves will ultimately approach the limiting configuration with a 120° angle at the crests.

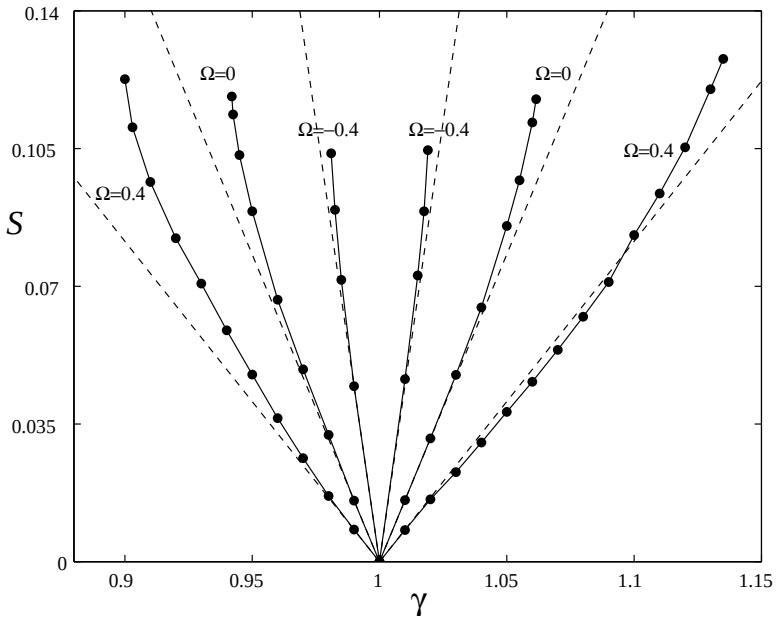

FIGURE 12. The dependence of the wave steepness S on the height of the plate γ for three different vorticity values $\Omega = -0.4$, 0, 0.4 when the Froude number is $F = 0.5$. The computed data is shown with the solid circles, while the linear steepness is shown with the dashed lines.

The reason why the nonlinear results for $\hat{F} = 0.5$, $\gamma = 0.99$ do not agree with the linear theory for vorticity values near $\Omega = -1$ can be found by considering the stagnation height $y_s = F^2(1+\Omega)^2/2 + 1$. As the vorticity decreases to $\Omega = -1$, the stagnation height also decreases, and approaches the undisturbed level $y = 1$. The elevation of the waves crests, however, can never be greater than the stagnation height, so nonlinear solutions can only exist for vorticities above some limiting value $\Omega^* > -1$. The free surface profiles for vorticity values just greater than Ω^* will have waves close to the limiting configuration, like the profile for $\Omega = -0.94$ in figure 13(a). For vorticity values much greater than Ω^*, the crests of the waves will no longer be close to the stagnation level, and the waves will appear to be sinusoidal in shape, agreeing with the linear theory.

A similar behaviour was found when we fixed $\hat{F} = 0.5$ and $\gamma = 0.95$. The solution profile for $\Omega = 0$ looks nonlinear in shape with broad troughs and sharp crests. These nonlinear characteristics of the free surface profiles increased as the vorticity decreased to $\Omega = -0.45$. No solutions with lower vorticity values could be computed, but again, as before with $\gamma = 0.99$, it is expected that the waves will soon break if the vorticity is decreased further. The solution profile for $\Omega = -0.45$ is shown in figure 13(b) as a dot-dashed line. As the vorticity increases from $\Omega = 0$, the solution profiles slowly

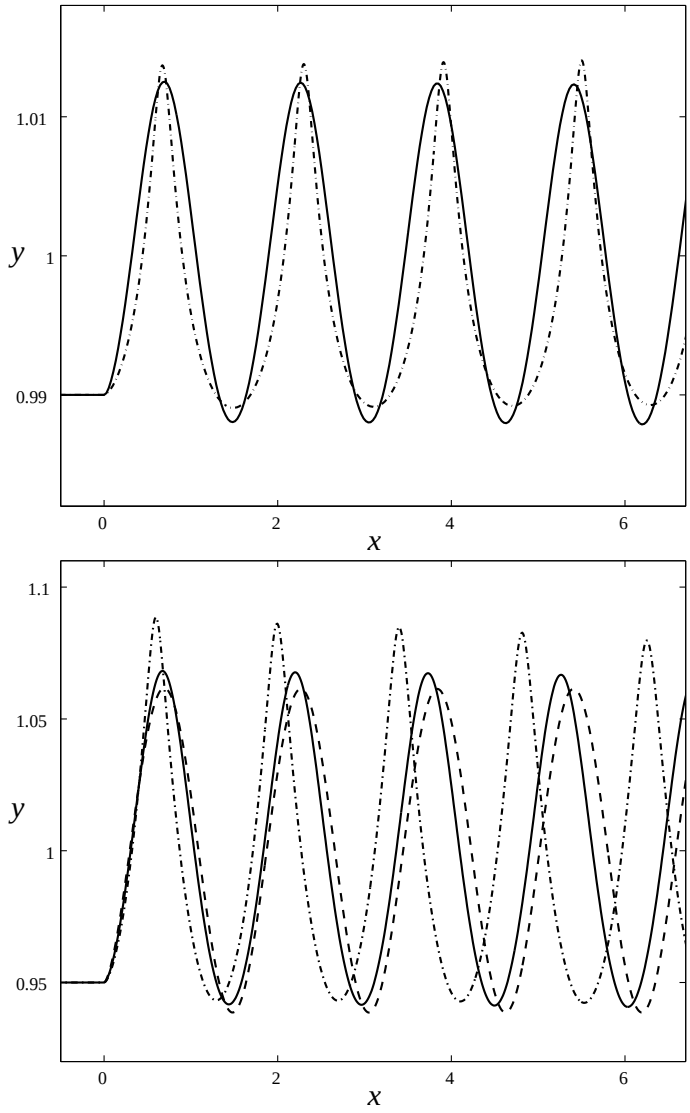

FIGURE 13. Typical free surface profiles for $\hat{F} = 0.5$. In (a), $\gamma = 0.99$. Here the solid profile corresponds to $\Omega = -0.7$ and $F = 1.325$, while the dot-dashed profile corresponds to $\Omega = -0.94$ and $F = 3.758$. In (b), $\gamma = 0.95$. Here the solid profile corresponds to $\Omega = 100$ and $F = 0.0057$, the dot-dashed profile corresponds to $\Omega = -0.45$ and $F = 0.828$, and the dashed line indicates the linear profile.

become more sinusoidal in shape. For all values of Ω greater than about 2, the shape of the free surface does not change. This constant shape for large vorticity values is easily distinguishable from the linear profile, as can be seen in figure 13(b) by comparing the solid profile for $\Omega = 100$ with the dashed linear profile. The fact that these profiles do not agree is to be expected, since $\gamma \not\approx 1$ in this case.

4. Summary

The steady free surface flow past a semi-infinite flat plate has been considered. With the use of conservation of mass and momentum, exact relationships between the Froude number, the plate height and the constant vorticity have been derived for the case where the downstream free surface is flat. This analysis has been made possible by the simple geometry of the problem. Complete nonlinear solutions to this wave-free problem have been calculated numerically with the use of a boundary integral method, and the results agree closely with the exact relationships. This agreement between exact and numerical results (see figures 2 and 5) shows that the boundary integral method computes solutions to a high degree of accuracy. It has been found that the introduction of a constant vorticity has led to some interesting behaviour not encountered previously in studies restricted to irrotational flow. Similar behaviour has been found in the study of solitary waves with constant vorticity (see, for example, Vanden-Broeck 1994; and Forbes & Belward (1996)). All the solutions computed without waves were supercritical downstream.

We have also considered solutions to the problem where the flow is characterized by a train of waves on the free surface. The behaviour of these subcritical solutions is completely different to that encountered in the wave-free problem. When the elevation of the plate is close to the level of the undisturbed free surface, the computed nonlinear solutions have been found to agree with linear solutions considered previously. This again confirms the accuracy of the numerical scheme. As the plate is moved away from the undisturbed level, the waves on the free surface become more nonlinear in shape, and ultimately approach limiting configurations with a 120° angle formed at the crests. The introduction of a constant vorticity here has not changed the qualitative behaviour of the solutions.

The work of the first author has been supported by a University of Queensland Postgraduate Research Scholarship.

REFERENCES

Asavanant, J. & Vanden-Broeck, J.-M. 1996 Nonlinear free-surface flows emerging from vessels and flows under a sluice gate. *J. Austral. Math. Soc.* B **38**, 63–86.

Benjamin, T. B. 1968 Gravity currents and related phenomena. *J. Fluid Mech.* **31**, 201–248.

Cokelet, E. D. 1977 Steep gravity waves in water of arbitrary uniform depth. *Phil. Trans. R. Soc. Lond.* A **286**, 183–230.

Dagan, G. & Tulin, M. P. 1972 Two-dimensional free-surface gravity flow past blunt bodies. *J. Fluid Mech.* **51**, 529–543.

Forbes, L. K. & Belward, S. R. 1996 Atmospheric solitary waves: some applications to the morning glory of the Gulf of Carpenteria. *J. Fluid Mech.* **321**, 137–155.

Kang, Y. & Vanden-Broeck, J.-M Stern waves with vorticity. *ANZIAM J.* (in press)

McCue, S. W. 1999 Two-dimensional bow and stern flows in a finite-depth fluid with constant vorticity. PhD thesis, University of Queensland, Brisbane, Australia.

McCue, S. W. & Forbes, L. K. 1999 Bow and stern flows with constant vorticity. *J. Fluid Mech.* **399**, 277–300.

McCue, S. W. & Forbes, L. K. 2001 Smoothly attaching bow flows with constant vorticity. *ANZIAM J.* **42**, 354–371.

McCue, S. W. & Stump, D. M. 2000 Linear stern waves in finite depth channels. *Q. J. Mech. Appl. Math.* **53**, 629–643.

Simmen, J. A. & Saffman, P. G. 1985 Steady deep-water waves on a linear shear current. *Stud. Appl. Math.* **73**, 35–57.

Teles da Silva, A. F. & Peregrine, D. H. 1988 Steep, steady surface waves on water of finite depth with constant vorticity. *J. Fluid Mech.* **195**, 281–302.

Vanden-Broeck, J.-M. 1980 Nonlinear stern waves. *J. Fluid Mech.* **96**, 603–611.

Vanden-Broeck, J.-M. 1994 Steep solitary waves in water of finite depth with constant vorticity. *J. Fluid Mech.* **274**, 339–348.

Vanden-Broeck, J.-M. & Keller, J. B. 1987 Weir flows. *J. Fluid Mech.* **176**, 283–293.